ISSN 0031-918X, Physics of Metals and Metallography, 2020, Vol. 121, No. 13, pp. 1258–1265. © Pleiades Publishing, Ltd., 2020.

STRUCTURE, PHASE TRANSFORMATIONS, AND DIFFUSION

Particle Dissolution and Recrystallization Progress of Al–Mg–Si–Cu Alloy during Solution Treatment

X. F. Wang[a, *], M. X. Guo[b], H. B. Wang[c], W. F. Peng[a], Y. G. Wang[a], J. S. Zhang[b], and L. Z. Zhuang[b]

[a] *Key Laboratory of Impact and Safety Engineering, Ministry of Education, Ningbo University, Ningbo, Zhejiang, 315211 China*

[b] *State Key Laboratory for Advanced Metals and Materials, University of Science and Technology Beijing, Beijing, 100083 China*

[c] *School of Materials Science and Engineering, Jiangxi University of Science and Technology, Ganzhou, Jiangxi, 341000 China*

**e-mail: wangxiaofeng@nbu.edu.cn*

Received June 10, 2019; revised September 10, 2019; accepted November 20, 2019

Abstract—Particle dissolution and recrystallization progress of Al–Mg–Si–Cu alloy during solution treatment at 555°C was studied by microstructure, hardness and electrical conductivity characterization, and analytical calculation in the present study. The results show that recrystallization and dissolution could occur concurrently during solution treatment, and the solution time has an appreciable influence on hardness, electrical conductivity, secondary phase particles and grain structure of the Al–Mg–Si–Cu alloy. As the solution time increases, the hardness decreases at first, and then increases, and almost remains constant finally; the electrical conductivity decreases sharply at first, and then decreases slowly, and almost keeps constant finally. In addition, the microstructure transforms from the deformation elongated bands to recrystallization equiaxed grains, and the particles are gradually dissolved with the increase of the solution time. The dissolution of the particles may be completed in the range of 120–300 s and the recrystallization was finished not exceeding 60 s. The predicted dissolution time by an analytical model combining classical diffusion-controlled dissolution equation for a single spherical particle and a John–Mehl–Avarami-like (JMA-like) equation is approximately 170 s, which is consistent with the experimental results.

Keywords: Al–Mg–Si–Cu alloy, microstructure, particle, dissolution, recrystallization

DOI: 10.1134/S0031918X20130189

INTRODUCTION

Currently, more and more attention is paid to the age-hardening Al–Mg–Si–Cu alloys used in automotive industry due to an excellent combination of service strength in the age hardened state and formability in the T4P state [1–5]. In general, solution treatment is very important to the manufacturing of Al–Mg–Si–Cu alloy sheet [6, 7], which plays a very important role in microstructure and mechanical properties controlling. During the solution treatment, two main changes could be found. On one hand, the elongated bands developed during cold rolling may transform to equiaxed grains as a result of the occurrence of recrystallization; on the other hand, a large number of soluble particles such as Mg_2Si, Si and $Al_{1.9}Mg_{4.1}Si_{3.3}Cu$ may be dissolved gradually [8]. Obviously, in order to take full advantage of the age hardening ability of Al–Mg–Si–Cu alloy, it is very essential to ensure enough solution time to dissolve all the soluble particles. However, too long solution time may result in coarse grain structure and strong texture, which are detrimental to the formability and mechanical properties. Accordingly, optimizing the solution time to dissolve all the soluble particles seems to be very important.

A dissolution process can be approximately regarded as a reversal of precipitation and is controlled by volume diffusion [9]. However, some authors [10, 11] have emphasized that dissolution is significant different from the precipitation. Two processes are involved in dissolution of a particle [12]: atomic transfer across the phase interface separating matrix and particle (interface diffusion), and diffusion of solute away from the interface (long-range diffusion). Over a period of many years, several models have been developed to describe the kinetics of particle dissolution in metals. Wang et al. [13] studied the dissolution kinetics of γ' particles in an binary Ni-Al alloys with different initial particle size distribution using a three dimensional quantitative phase field model and found that the volume fraction of particles decays exponentially with time during dissolution, irrespective of the initial particle size distribution, but the dissolution rate depends strongly on the initial particle size distribution. Ferro [14] proposed a semi-empirical model for isothermal particle dissolution to predict the isothermal dissolution of σ phase in duplex stainless steel, and the analytical results agree with the experimental results very well. Nojiri and Ennmoto [15] calculated the dissolution of spherical particles in an infinitely

large matrix by a numerical method. Zuo et al. [16] proposed an analytical model for dissolution kinetics of particles upon isothermal annealing, which considers the interactions of solute diffusion fields in front of the secondary phase/matrix interface upon dissolution and predicted the isothermal dissolution of θ' in an Al–3.0 wt %–Cu alloy and silicon particles in Al–0.8 wt %–Si alloy successfully. Zhang et al. [17] proposed a similar analytical model, which is used to deal with dissolution process for different kinds of precipitations in Al–Mg–Si–Cu alloys and the prediction agrees the experimental results well.

Considering the importance of solution treatment, it is essential to understand the dissolution behavior of particles and microstructure transformation of Al–Mg–Si–Cu alloy during solution treatment. However, there is still lack of related study. Accordingly, in the present study, particle dissolution and recrystallization progress of Al–Mg–Si–Cu alloy during solution treatment was studied systematically, and the goal is to clarify the relationship between particle dissolution and recrystallization progress. Hopefully, this work could provide a guide to optimize the solution treatment parameter.

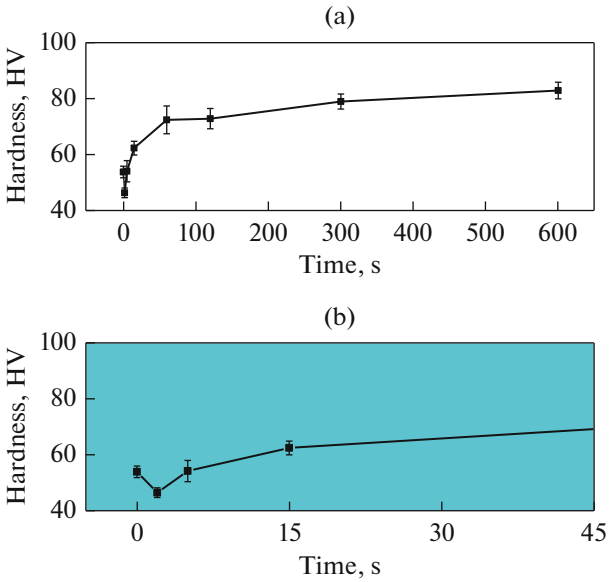

Fig. 1. Vickers hardness of the solution treated Al–Mg–Si–Cu alloy for different times: (a) overall presentation; (b) local details.

EXPERIMENTAL

The received material was a cold-rolled Al–Mg–Si–Cu alloy sheet (Al–0.8Mg–0.9Si–0.2Cu–0.1Mn (wt %)) with a thickness of 1 mm. Since Fe-rich phase particles will not be dissolved during solution treatment, in order to observe the transformation of the soluble particles more accurately, no Al–Fe master alloy was prepared for the alloy. In order to investigate the particle dissolution and recrystallization progress, the alloy sheet was divided into several parts and they were solution treated in a salt bath furnace at 555°C for different times (2, 5, 15, 60, 120, 300, and 600 s).

Hardness and electrical conductivity measurements were conducted on the solution treated specimens for different solution times. Vickers micro-hardness measurements were carried out on the longitudinal sections of the specimens using a Wolpert-401MVD Vickers hardness tester under a load of 200 g for the holding time of 30 s. Electrical conductivity was measured by an eddy current electro-conductive machine 7501A. Electrical conductivity was represented in the unit of %ICAS (International Annealed Copper Standard).

Microstructure of the cold-rolled alloy sheet and solution treated alloy sheets for different times were investigated through a Carl ZEISS Axio Imager A2m optical microscope (OM). The particle distribution of the cold-rolled Al–Mg–Si–Cu alloy was conducted through a SUPRA 55 field emission scanning electron microscope (SEM) equipped with X-ray energy dispersive spectrometers (EDS) systems. Particle distributions of the solution treated alloy sheets for different times were investigated using a TecnaiG2 F30 transmission electron microscope (TEM) equipped with X-ray energy dispersive spectrometer (EDS) systems. Thin foils for TEM studies were first mechanically grinded to a thickness of 100 μm, and then twin-jet polished in a solution of 30% nitric acid and 70% methanol at a temperature of –25°C.

RESULTS AND DISCUSSION

Figure 1 presents Vickers hardness of the alloy sheets solution treated for different times (0, 2, 5, 15, 60, 120, 300, and 600 s). As can be seen, there is no monotonic relationship between hardness and solution time. It is very interesting that as the solution time increases, the hardness decreases at first, and then increases, and almost remains constant finally. When the solution time is 2 s, the hardness decrease significantly, indicating the recrystallization has occurred; when the solution time is in the range of 2–60 s, the hardness increases appreciably. Obviously, solution strengthening is the main strengthening mechanism. When the solution time is in the range of 60–600 s, the hardness changes slightly, revealing that the particle dissolution may be almost completed by the solution time of about 60 s. However, the conclusion about dissolution time from hardness tests is rough, therefore, electrical conductivity tests were performed.

Electrical conductivities of the alloy sheets solution treated for different times (0, 2, 5, 15, 60, 120, 300, and 600 s) are revealed in Fig. 2. It can be found that the electrical conductivity-time curve is different from the hardness-time curve. As the solution time increases, electrical conductivity decreases sharply at first, and then decreases slowly, and almost keep constant finally. This should be related to the dissolution of par-

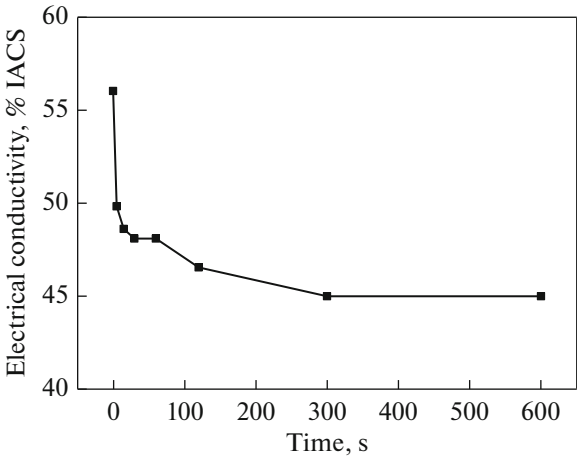

Fig. 2. Electrical conductivity of the solution treated Al–Mg–Si–Cu alloy for different times.

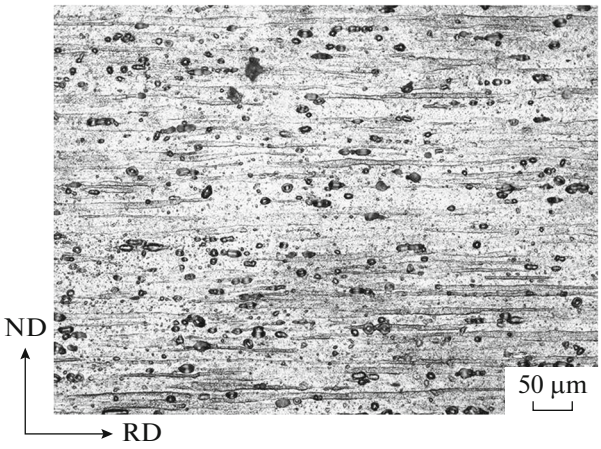

Fig. 3. Microstructure of the cold-rolled Al–Mg–Si–Cu alloy.

ticles and recrystallization progress. As is well known, recrystallization could result in the improvement of electrical conductivity, on the contrary, the dissolution of particles is detrimental to electrical conductivity as a result of the lattice distortion effect. Accordingly, the competition between recrystallization and dissolution of particles determines the electrical conductivity. When the solution time reaches 2 s, the electrical conductivity decreases sharply, indicating the strong dissolution has occurred at the very early stage of solution treatment; when the solution time is in the range of 120–300 s, the electrical conductivity decreases slowly; when the solution time is more than 300 s, electrical conductivity changes slightly, implying that the dissolution of the particles may be completed in the range of 120–300 s.

Based on the above analysis, it can be found that hardness and electrical conductivity could reflect the dissolution behavior and recrystallization progress in some extent. However, different conclusions about dissolution time are obtained according to hardness tests and electrical conductivity tests. Accordingly, it is essential to observe the microstructure variation with the solution time. And the representative alloy sheets solution treated for 5, 15, 60, and 120 s were selected to investigate their microstructure.

Figure 3 shows the microstructure of the cold-rolled Al–Mg–Si–Cu alloy sheet. As can be seen, the typical deformation elongated bands along rolling direction (RD) are dominant in the alloy matrix.

The particle distribution of the cold-rolled Al–Mg–Si–Cu alloy sheet is presented in Fig. 4. There are two kinds of particles with different colors in the alloy matrix. According to EDS analysis, the white particles with the size exceeding 1 μm are identified as Al(Fe,Mn)Si and the black finer particles are identified as Mg_2Si. Interestingly, very few non-soluble Al(Fe,Mn)Si particles can still be observed, indicating that the high-purity aluminum includes very low content of Fe. The weight ratio of Mg and Si is 0.89, therefore, the alloy should be a Si-excess Al–Mg–Si–Cu alloy. In addition, the solubility of Si at room temperature is only 0.05 wt%. Accordingly, Si particles should also be in the matrix.

In order to confirm the conclusion, TEM analysis is conducted on the alloy, as revealed in Fig. 5. It can be seen that many particles distribute in the alloy matrix and the EDS results prove that the lath-shaped particles are Al(Mg,Si)Cu and the large global particles are Si. The previous study has revealed that Al(Mg,Si)Cu is $Al_{1.9}Mg_{4.1}Si_{3.3}Cu$ (Q) [18]. Based on the observations, there are four types of particles in the alloy matrix.

Recrystallization microstructure of the alloy sheets solution treated for different times is shown in Fig. 6. As can be observed, their recrystallization microstructure is different. The alloy sheet solution treated for 5 s possesses elongated coarse grains and fine equiaxed grains. After that, as the solution time increases, more and more equiaxed grains are developed and the grain size distributions become uniform gradually. When the solution time reaches 60 s, the microstructure is almost comprised of the equiaxed grains, indicating all the deformation microstructure is replaced by the recrystallization microstructure. Furthermore, grains tend to grow appreciably when the solution time reaches 120 s. According to the microstructure transformation characterization, it can be inferred that the recrystallization was finished with the solution time not exceeding 60 s. Notably, when the solution time reaches 120 s, the coarse grain structure could result in the decrease of the hardness. As previously mentioned, when the solution time is in the range of 60–600 s, the hardness changes slightly. Consequently, the fact implies that the dissolution of the particles could not be completed by the solution time of 60 s. The combined effect of recrystallization grain growth and dissolution of the particles results in the almost constant hardness.

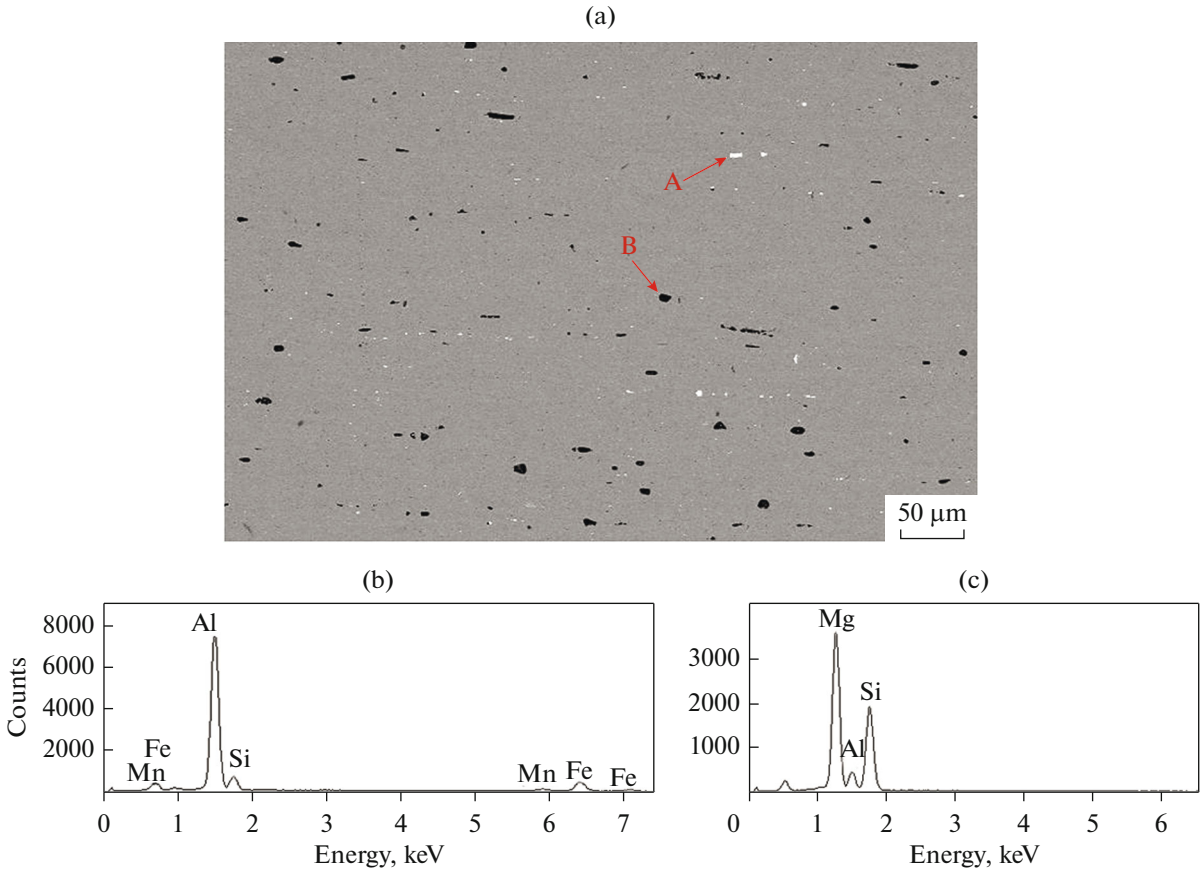

Fig. 4. SEM analysis of the cold-rolled Al–Mg–Si–Cu alloy: (a) particle distribution; (b), (c) EDS spectra of the particles.

Particle transformations of the Al–Mg–Si–Cu alloy during solution treatment are shown in Fig. 7. As can be seen, most of the particles are global, and the particles decreases gradually with the increase of the solution time. When the solution time reaches 120 s, some particles are still in the alloy matrix. On the basis of the above analysis, the solution time of 120 s is not enough to remove all the soluble particles, so the particles should be comprised of the non-soluble Al(Fe,Mn)Si and other soluble particles.

DISSOLUTION KINETICS

As mentioned in Introduction part, Zhang et al. [17] used an analytical model to predict the dissolution kinetics successfully. In this part, the model is also applied to calculate the dissolution kinetics. The model is considered as a combination of the classical diffusion-controlled dissolution equation for a single spherical particle and a JMA-like equation. In order to obtain more accurate results, the model considers the interactions of adjacent particles and is derived based on the following assumptions: (1) all the particles could be approximately seen as sphere shape of the same size; (2) the chemical composition of the particles will not change during the dissolution process; (3) solid solubility and diffusion coefficient of each element will keep unchanged; (4) the JMA-like equation is applicable during the dissolution process. More details about this model can refer to [15, 16].

According to this model, the relationship between dissolution degree and solution time can be expressed as

$$\frac{R_{tm}^3}{R_0^3} = 1 - m(1 - \exp(-x_e)), \tag{1}$$

where R_0 and R_{tm} are the initial radius of the particle and the radius of particle at t_m, respectively, m is a modified proportional factor and equal to $e/(e-1)$, x_e stands for the extended transformed fraction and can be expressed as

$$x_e = \frac{1}{R_0^3} \times \left\{ \begin{array}{l} {}^3R_0\left(\sqrt{\frac{k}{\pi}}\right)\left(R_1 - \sqrt{\frac{kDt_m}{m}}\right) + \sqrt{R_1^2 - \frac{kDt_m}{m}} \\ \times\left(\frac{\sqrt{kDt_m}}{\sqrt{m}R_1 + \sqrt{mR_1^2 - kDt_m}} + \sqrt{\frac{k}{\pi}}\right)\left(\frac{kDt_m}{m}\right)^{1/2} \\ + \left(\frac{\sqrt{kDt_m}}{\sqrt{m}R_1 + \sqrt{mR_1^2 - kDt_m}} + \sqrt{\frac{k}{\pi}}\right)^3\left(\frac{kDt_m}{m}\right)^{3/2} \end{array} \right\}, \tag{2}$$

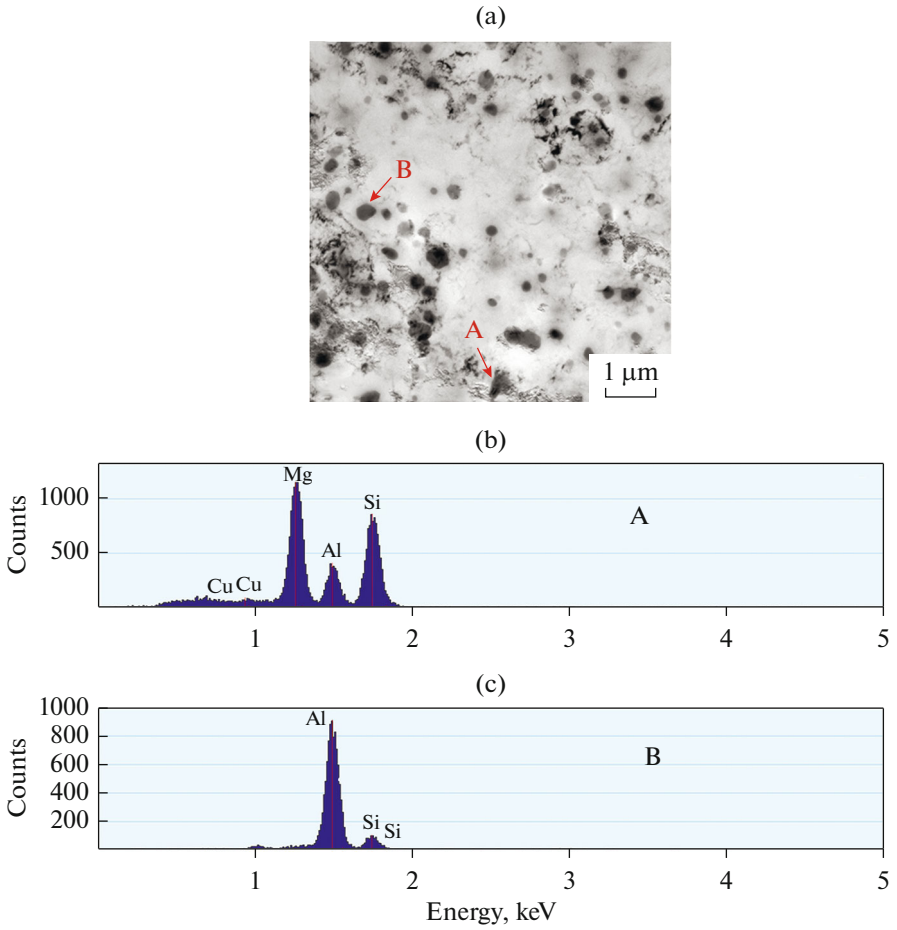

Fig. 5. TEM analysis of the cold-rolled Al–Mg–Si–Cu alloy: (a) particle distribution; (b), (c) EDS spectra of the particles.

$$k = \frac{2\left(C^{\alpha/\beta} - C^{m}\right)\frac{\rho_\alpha}{M_\alpha}}{C^{\beta/\alpha}\frac{\rho_\beta}{M_\beta} - C^{\alpha/\beta}\frac{\rho_\alpha}{M_\alpha}}, \quad (3)$$

$$D = D_0 \exp\left(-\frac{Q}{R_g T}\right), \quad (4)$$

$$R_l = \frac{1}{\left(1 + \sqrt{\frac{k}{\pi}}\right)} R_0, \quad (5)$$

where k is dimensionless parameter, $C^{\alpha/\beta}$, $C^{\beta/\alpha}$ and C^{m} represent the atom solid solubility (wt %) at solution temperature, the atom concentration (wt %) in the particle near the interface and the initial atom concentration (wt %) in the matrix, respectively, ρ_α and ρ_β stand for the average density of α matrix and β precipitate, respectively, M_α and M_β, respectively, are the average molar mass of α matrix and β precipitate, D is the diffusion coefficient at the solution temperature, D_0 is the pre-exponential factor, Q is the activation energy, R_g is the gas constant, T is the absolute temperature.

According to theses equations, it could be found that the theoretic dissolution time of the particles can be calculated by substituting the parameters, and it could be affected by many factors such as particle size, chemical composition. The previous study [18] has confirmed that Si particles may take the longest time to be completely dissolved than other soluble particles such as Mg_2Si and Q. In addition, Al(Fe, Mn)Si particles could not be dissolved during solution treatment. Therefore, in the present study, the complete dissolution time of these soluble particles could be approximately considered as the dissolution time of Si particles. The calculation parameters of Si particles are listed in Table 1. The initial solute concentration of the alloy in Al matrix is about 0.7 wt %, according to EDS quantity analysis of alloy matrix.

According to the Matlab R2013a software, variation of the dissolution degree with solution time could be obtained. Figure 8 shows the effect of the particle radius on the dissolution time of Si particles at 555°C. As can be seen, the dissolution time of Si particles is significantly by particle size, and it increases with

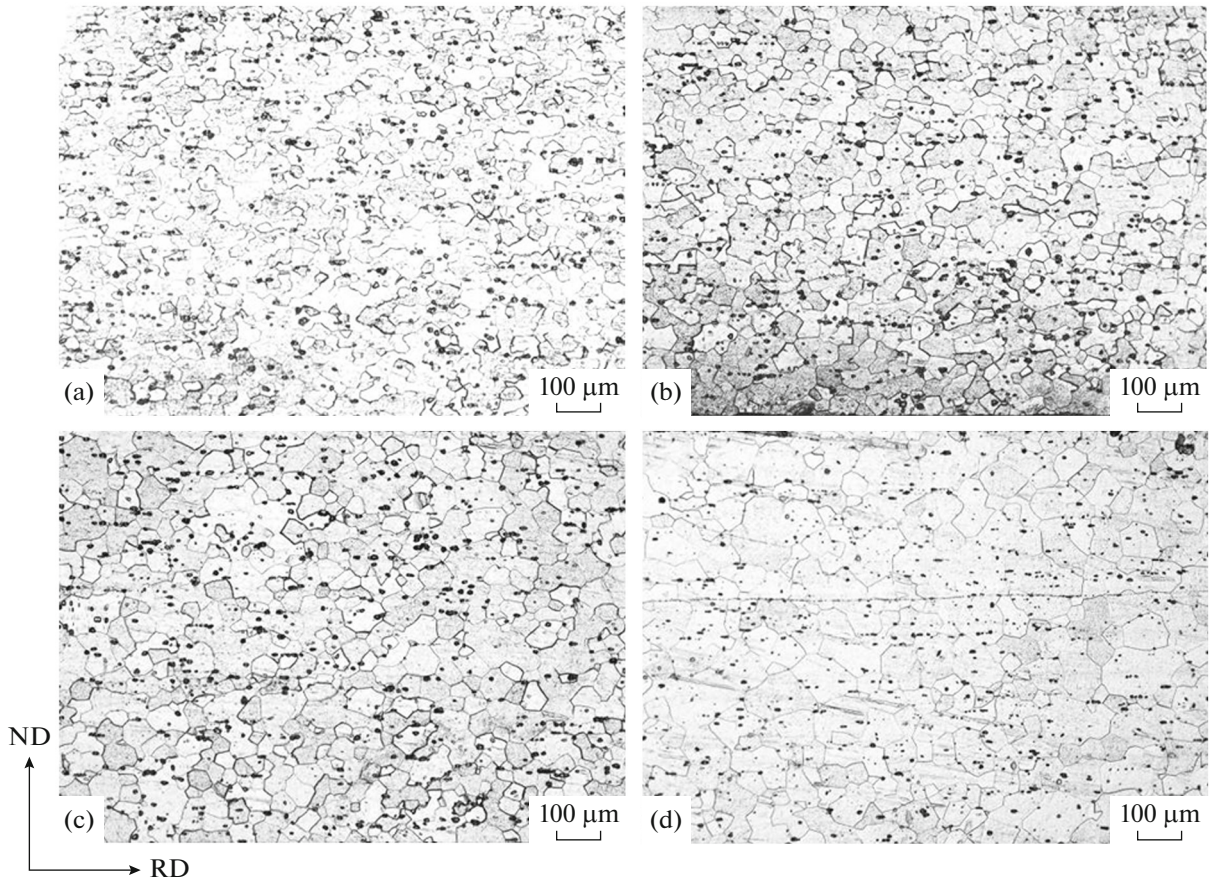

Fig. 6. Microstructure of the solution treated Al–Mg–Si–Cu alloy for different times: (a) 5; (b) 15; (c) 60; (d) 120 s.

increasing particle radius. As can be seen in Fig. 5, the cold-rolled alloy sheet contains many particles with a wide size range. In order to dissolve all the soluble particles, the complete dissolution time could be approximately considered as the dissolution time of the relatively large particles with a radius of 0.5 μm. Therefore, the alloy sheet needs 170 s to dissolve them theoretically. The previous experimental results also have revealed that the complete dissolution time should be in the range of 120–300 s. The predicted results are consistent with the experimental results. Accordingly, it is reasonable to predict the dissolution time by the model.

The above experimental and calculation results have suggested that recrystallization and dissolution could occur concurrently during solution treatment. Compared with recrystallization, the dissolution of the particles may take longer time. The concurrent dissolution and recrystallization may have a significant influence on the mechanical property, especially the deep drawability. Therefore, it is reasonable to optimize the deep drawability through controlling the dissolution of particles and recrystallization progress. As is commonly accepted [19, 20], texture is greatly affected by the particles. During solution treatment, coarse particles are beneficial to the formation of weak recrystallization texture, while fine particles tend to develop strong Cube texture. The former is beneficial to the deep drawability, while the latter is detrimental to the deep drawability. Obviously, the weak texture could be obtained by the solution time controlling to adjust the particle size, thus, this may result in the excellent deep drawability. The subject will be studied systematically in future.

Table 1. Parameters of Si particles used for analytical calculations [15, 16]

Paramter	Value
$C^{\alpha/\beta}$, wt %	1.27
$C^{\beta/\alpha}$, wt %	100
$\frac{\rho_\alpha}{M_\alpha}$, mol/m^3	1×10^5
$\frac{\rho_\beta}{M_\beta}$, mol/m^3	8.36×10^4
Q, kJ/mol	139
D_0, m^2/s	9×10^{-5}

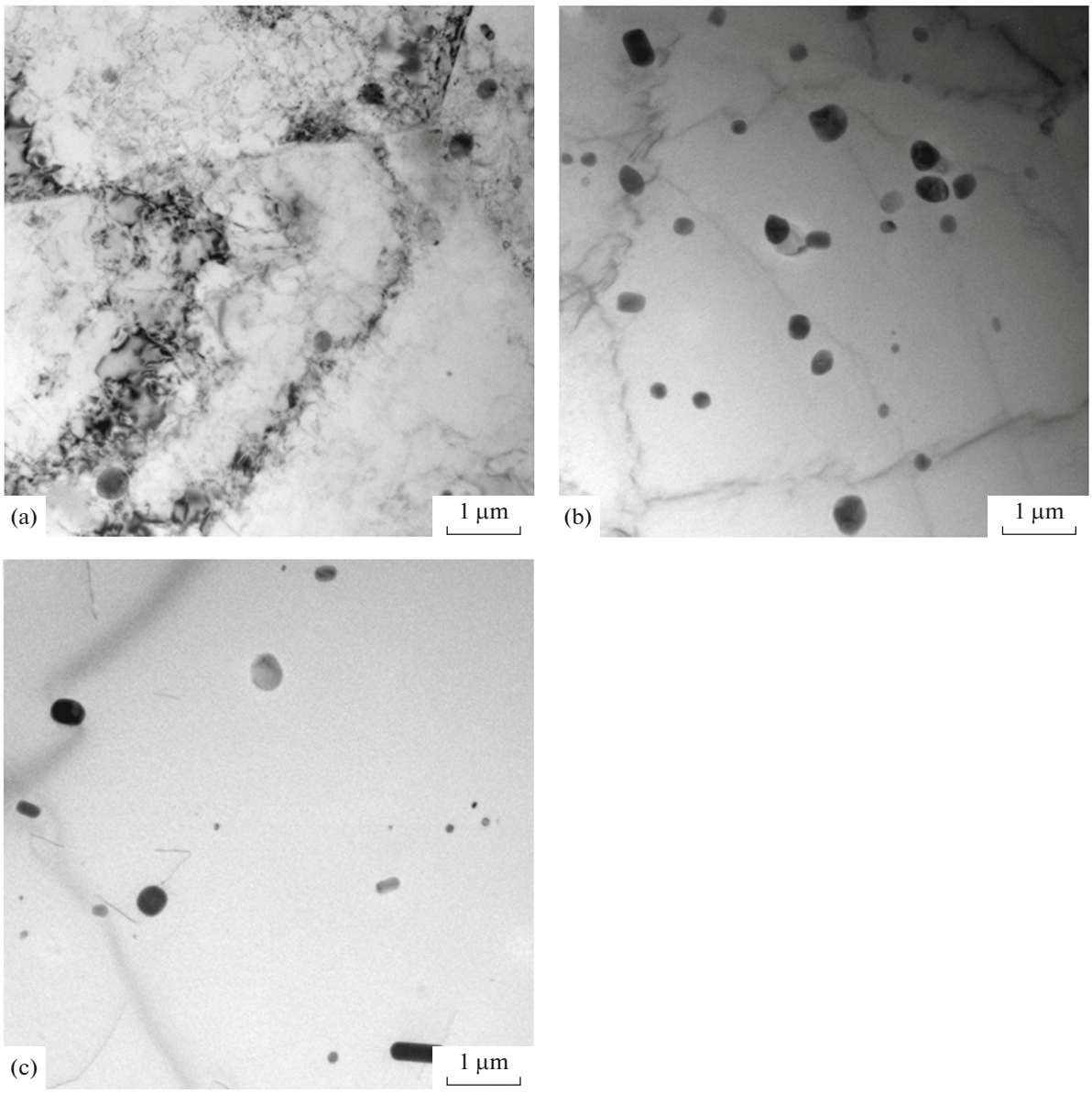

Fig. 7. TEM micrographs of solution treated Al–Mg–Si–Cu alloy for different times: (a) 5; (b) 15; (c) 120 s.

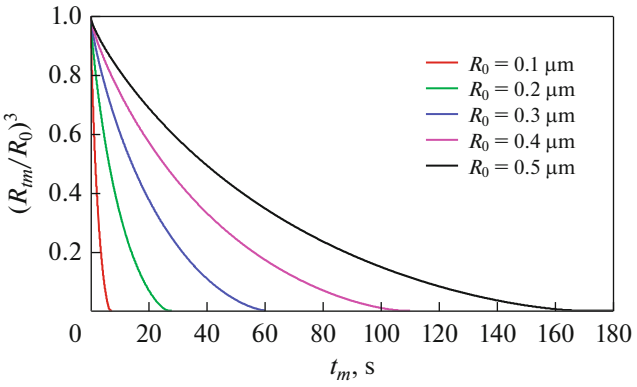

Fig. 8. Relationship between $(R_{tm}/R_0)^3$ and t_m for Si particles with different sizes.

CONCLUSIONS

Particle dissolution and recrystallization progress of Al–Mg–Si–Cu alloy during solution treatment has been systematically studied. The following results are drawn from this research.

(1) Solution time has a significant influence on hardness and electrical conductivity. As the solution time increases, the hardness decreases at first, and then increases, and almost remains constant finally; the electrical conductivity decreases sharply at first, and then decreases slowly, and almost keeps constant finally.

(2) Microstructure is significantly affected by solution time. Recrystallization and dissolution could occur concurrently in the alloy sheet during solution

treatment. As the solution time increases, the microstructure transforms from the deformation elongated bands to recrystallization equiaxed grains, and the equiaxed grains have a continuous growth. In addition, the particles are gradually dissolved with the increase of the solution time.

(3) An analytical model combining classical diffusion-controlled dissolution equation for a single spherical particle and a John–Mehl–Avarami-like (JMA-like) equation is used to predict the dissolution time of the particles. The complete dissolution time is approximately 170 s, which is consistent with the experimental results. Accordingly, the model could be used to optimize solution treatment.

FUNDING

This work was supported by the National Key Research and Development Program of China under grant no. 2016YFB0300801 the Opening Project of State Key Laboratory for Advanced Metal Material under grant no. 2019-Z02 and National Science Foundation of China under grant no. 52075272; the Science Challenge Project under grant no. TZ2018001; Zhejiang Provincial Natural Science Foundation of China under grant no. LQ17E010001; Ningbo Natural Science Foundation under grant no. 2018A610174; Natural Science Foundation of Ningbo University under grant no. XYL18017 and the K.C. Wong Magna Fund from Ningbo University.

REFERENCES

1. W. S. Miller, L. Zhuang, J. Bottema, A. J. Wittebrood, P. De Smet, A. Haszler, and A. Vieregge, "Recent development in aluminium alloys for the automotive industry," Mater. Sci. Eng., A **280**, 37–49 (2000).
2. J. Hirsch, "Recent development in aluminium for automotive applications," Trans. Nonferrous Met. Soc. China **24,** 1995–2002 (2014).
3. A. Yu. Churyumov, A. V. Mikhailovskaya, A. D. Kotov, A. I. Bazlov, and V. K. Portnoi, "Developement of mathematical models of superplasticity properties as a function of parameters of aluminum alloys of Al–Mg–Si system," Phys. Met. Metallogr. **114**, 272–278 (2013).
4. J. Hirsch and T. Al-Samman, "Superior light metals by texture engineering: Optimized aluminum and magnesium alloys for automotive applications," Acta Mater. **61**, 818–843 (2013).
5. X. W. Ren, Y. C. Huang, and Y. Liu, "Effect of homogenization on microstructure and properties of Al–Mg–Si roll-casting sheet," Phys. Met. Metallogr. **119**, 789–796 (2018).
6. O. Engler and J. Hirsch, "Texture control by thermomechanical processing of AA6xxx Al–Mg–Si sheet alloys for automotive applications-a review," Mater. Sci. Eng., A **336,** 249–262 (2002).
7. X. F. Wang, M. X. Guo, C. Q. Ma, J. B. Chen, J. S. Zhang, and L. Z. Zhuang, "Effect of particle size on the microstructure, texture, and mechanical properties of Al–Mg–Si alloy," Int. J. Miner. Metall. Mater. **25**, 957–966 (2018).
8. X. F. Wang, M. X. Guo, L. Y. Cao, J. R. Luo, J. S. Zhang, and L. Z. Zhuang, "Effect of heating rate on mechanical property, microstructure and texture evolution of Al–Mg–Si–Cu alloy during solution treatment," Mater. Sci. Eng., A **621**, 8–17 (2015).
9. G. Thomas and M. J. Whelan, "Observations of precipitation in thin foils of aluminium +4% copper alloy," Philos. Mag. **6**, 1103–1114 (1961).
10. H. B. Aaron, D. Fainstein, and G. R. Kotler, "Diffusion-limited phase transformations: a comparison and critical evaluation of the mathematical approximations," J. Appl. Phys. **41**, 4404–4410 (1970).
11. M. J. Whelan, "On the kinetics of precipitate dissolution," Met. Sci. J. **3**, 95–97 (1968).
12. L. C. Brown, "Diffusion controlled dissolution of planar, cylindrical, and spherical precipitates," J. Appl. Phys. **47**, 449–458 (1976).
13. G. Wang, D. S. Xu, N. Ma, N. Zhou, E. J. Payton, R. Yang, M. J. Mills, and Y. Wang, "Simulation study of effects of initial particle size distribution on dissolution," Acta Mater. **57**, 316–325 (2009).
14. P. Ferro, "A dissolution kinetics model and its application to duplex stainless steels," Acta Mater. **61**, 3141–3147 (2013).
15. N. Nojiri and M. Enomoto, "Diffusion-controlled dissolution of a spherical precipitate in an infinite binary alloy," Scr. Metall. Mater. **32**, 787–791 (1995).
16. Q. Zuo, F. Liu, L. Wang, C. F. Chen, and Z. H. Zhang, "An analytical model for secondary phase dissolution kinetics," J. Mater. Sci. **49**, 3066–3079 (2014).
17. X. K. Zhang, M. X. Guo, J. S. Zhang, and L. Z. Zhuang, "Dissolution of precipitates during solution treatment of Al–Mg–Si–Cu alloys," Metall. Mater. Trans. B **47**, 608–620 (2016).
18. X. F. Wang, M. X. Guo, A. Chaupis, J. R. Luo, J. S. Zhang, and L. Z. Zhuang, "Effect of solution time on microstructure, texture and mechanical properties of Al–Mg–Si–Cu alloys," Mater. Sci. Eng., A **644**, 137–151 (2015).
19. O. Engler and J. Hirsch, "Recrystallization textures and plastic anisotropy in Al–Mg–Si sheet alloys," Mater. Sci. Forum **217–222**, 479–486 (1996).
20. R. D. Doherty, D. A. Hughes, F. J. Humphreys, J. J. Jonas, D. Juul Jensen, M. E. Kassner, W. E. King, T. R. McNelley, H. J. McQueen, and A. D. Rollett, "Current issues in recrystallization: a review," Mater. Sci. Eng., A **238**, 219–274 (1997).